

Fluorescence of Single Rhodamine Molecules Near the Surface of Gold

Liping Fang,* Haolin Li, Xuhang Ma, Qiuming Song, Xi Zhu, and Rui Chen*

Fluorescent properties of single Rhodamine molecules at different distances to the surface of a high-quality polycrystalline gold film are investigated by the time-correlated single-photon counting technique. The fluorescence lifetime and the fluorescence intensity of the dye molecules as a function of their distance to the gold surface are modeled quantitatively by a classical model for a horizontal electric dipole. The analysis shown herein represents a useful tool to model and further to control molecular fluorescence near complex plasmonic structures, where delicate manipulation of fluorescence emission intensity is of paramount importance.

enhanced fluorescence signal could be detected when the fluorophores are placed near well-designed plasmonic platforms, namely, the metal-enhanced fluorescence (MEF) effect.^[5,6] By introducing the plasmonic platform, the excited state of the fluorophore experiences an additional electric field, i.e., the near field of the plasmonic resonance, allowing the fluorophore to radiate more fluorescent photons.^[8,9] Before embarking on the investigation of such advanced plasmonic structures, it is essential to study and understand the fluorescent behavior of dipole-like emitters near the surface of metallic surfaces.^[13–15]

1. Introduction

Tuning the spontaneous emission of dipole-like quantum emitters with metallic structures is attractive to many fields such as single-photon source for future quantum technology^[1–4] and surface-enhanced fluorescence for life science and biotechnology.^[5–9] Novel metallic structures which support unique plasmonic resonance can offer unprecedented properties for a variety of application fields.^[10–12] For example, significantly

Drexhage pioneered such studies by investigating the fluorescence lifetime of an europium complex as a function of its distance to gold, silver, and copper mirrors.^[16] The distance between the europium complex and the metallic mirrors, as well as the monolayer of europium complex, were obtained by the sophisticated Langmuir–Blodgett technique.^[17–19]

In this work, we investigate fluorescent properties of Rhodamine 6G molecules at different distances to the surface of gold simply by spin coating of the dye molecules at different distances to a gold film. Our sample structure is similar to Drexhage's; however, our experimental approaches are much simpler. We show that fluorescence lifetimes of the Rhodamine 6G molecules at different distances to the gold film can be well explained by a classical dipole model developed by Chance, Prock, and Silbey (CPS).^[20] A quantum mechanical equivalence has been obtained by introduction of the local density of states (LDOS) of the electromagnetic waves.^[21,22] Upon fitting of the fluorescence lifetimes to the CPS model, the fluorescent quantum yield and intrinsic fluorescence lifetime of the emitter can be obtained. Such kind of distance-dependency study on metallic surface is able to obtain the quantum yield and intrinsic fluorescence lifetime of dipole-like quantum emitters,^[2,23,24] and applications can be found in nanometric distance rulers^[25–27] and nanopositioning of molecules in biosystems.^[28,29] Furthermore, we calculated the probability to detect fluorescence in the far field among other power dissipation channels of the dipole radiation, such as trapping in the silicon oxide waveguide and energy transfer to the gold film. We find that the modeled fluorescence probability fits well with the measured fluorescence intensity of the Rhodamine molecules at different distance to the gold surface. Our work paves way for further investigation of light–matter interactions incorporating advanced plasmonic structures and emerging low dimensional materials.^[30–32]


L. Fang, X. Zhu
School of Science and Engineering
The Chinese University of Hong Kong
Shenzhen 518172, P. R. China
E-mail: fangliping@cuhk.edu.cn

L. Fang, H. Li, R. Chen
Department of Electrical and Electronic Engineering
Southern University of Science and Technology
Shenzhen 518055, P. R. China
E-mail: chenr@sustech.edu.cn

H. Li
State Key Laboratory of High Power Semiconductor Laser
School of Science
Changchun University of Science and Technology
Changchun 130022, P. R. China

X. Ma
Core Research Facilities
Southern University of Science and Technology
Shenzhen 518055, P. R. China

Q. Song
College of New Materials and New Energies
Shenzhen Technology University
Shenzhen 518118, P. R. China

 The ORCID identification number(s) for the author(s) of this article can be found under <https://doi.org/10.1002/pssb.202200025>.

DOI: 10.1002/pssb.202200025

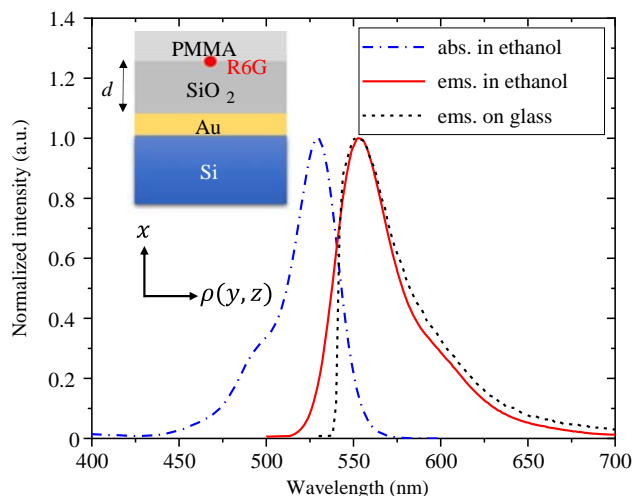


Figure 1. Absorption (abs.) and emission (ems.) spectra of Rhodamine 6G in ethanol solution and on glass substrate. Inset: sample structure under investigation.

2. Experimental Section

The sample structure is shown in **Figure 1**. First, a 100 nm-thick gold film was evaporated on silicon, and then silicon oxide of variable thickness d was deposited by plasma-enhanced chemical vapor deposition (PECVD). Then Rhodamine 6G molecules were spin-coated on the silicon oxide spacer layer and finally a protective 70 nm-thick polymethyl methacrylate (PMMA) layer was deposited atop.

The 100 nm-thick gold film was deposited on a 4 inch silicon wafer by electron beam evaporation (HHV TF500 box coater) at high vacuum (5×10^{-6} Torr) and room temperature. During deposition the silicon wafer was rotated at the rate of 20 round per minute (rpm). To enhance adhesion, a 5 nm-thick chromium layer was predeposited on silicon. The thickness of the metal film was monitored by a quartz crystal oscillator (Inficon SQC-310) and verified by profilometry (KLA Tencor P-7 stylus profiler), X-ray reflectivity (XRR, Rigaku SmartLab X-ray diffractometer, copper $K\alpha$ line at 1.54059 \AA , scanning angle range $2\theta = 0\text{--}10^\circ$, and step size 0.01°), and field-emission scanning electron microscopy (FESEM, Zeiss GeminiSEM 300) measurements. The deposition was maintained at a low rate of 2 \AA s^{-1} to obtain a smooth surface. The surface roughness of the gold surface was characterized by atomic force microscopy (AFM, Asylum Research MFP-3D-SA) in the tapping mode. The crystalline structure of the gold film was measured by the X-ray diffractometer in the θ - 2θ mode with scan step of 0.02° . The resistivity of the gold surface was measured by a four-point probe (Four Dimensions 280SI). The refractive index of the gold surface was characterized by variable angle spectroscopic ellipsometry (VASE, J. A. Woollam M2000VI) in the spectral range of 370–1690 nm.

The silicon wafer with gold film was then diced to $15 \times 15 \text{ mm}^2$ pieces before the deposition of silicon oxide spacer layers in the PECVD chamber. The oxide films were deposited using standard recipe optimized by the manufacturer (Oxford

Instruments PlasmaPro80). To calibrate the silicon oxide film thickness on gold surface, reference silicon pieces without gold film were also loaded to the chamber. The deposition rate of silicon oxide was around 1 nm s^{-1} and the temperature of the substrate was maintained at 300°C . The deposition times of the silicon oxide films are 1.1 times the nominal film thickness (20, 50, 100, 150, 200, 250, 300, and 350 nm). Submonolayer of Rhodamine 6G dye molecules was obtained on silicon oxide surface by spin coating (LEBO Science AC200-SE) $50 \mu\text{L}$ of a highly diluted alcohol solution of the dye ($1 \times 10^{-4} \text{ mol L}^{-1}$) at the speed of 3000 rpm for 60 s.^[33,34] Finally, a protective layer of PMMA with thickness around 70 nm was deposited atop by spin coating $50 \mu\text{L}$ of 2% anisole solution of PMMA (MicroCHEM NANO 950PMMA). The refractive index and film thickness of the silicon oxide and PMMA films were measured by VASE.

The fluorescence emission spectrum and fluorescence lifetime of the samples were characterized by the time-correlated single photon counting technique (TCSPC) using a time-resolved fluorescence spectrometer (PicoQuant FluoTime 300). For fluorescence lifetime measurements, the excitation laser was a 512 nm diode laser (PicoQuant LDH-P-C-520) working at the repetition rate of 20 MHz. The laser intensity is 0.45 mW and the beam size is approximately 1 mm. Fluorescence decays were recorded at the wavelength of 600 nm to avoid intermolecular energy transfer. For fluorescence emission spectrum measurements, the TCSPC system was switched to the steady-state mode. The molecules were excited by a diode laser (PicoQuant LDH-P-C-450B) with central wavelength at 455 nm and repetition frequency of 40 MHz. The laser intensity is 5.1 mW and the beam size is approximately 1 mm. More details of the optical configurations of the TCSPC system could be found in our previous work.^[35]

3. Results and Discussion

3.1. Gold Film Properties

The various properties of the gold film deposited on silicon substrate were characterized by XRD(R), AFM, SEM, and profilometry. The thickness of the gold film was measured by profilometry, XRR, and FESEM. **Figure 2** shows the step profile of the 100 nm-thick gold film on a silicon substrate. The inset shows the cross-sectional view of the gold film which has already been covered by a 200 nm-thick silicon oxide layer, as revealed by FESEM.

The XRR result is shown in Figure S1, Supporting Information. The thickness of the gold film is close to 100 nm. This result is consistent with the film thickness revealed by FESEM and profilometry. The XRR measurement indicates that the density of the gold film is $19.4 \pm 0.3 \text{ g cm}^{-3}$, which is similar to bulk gold.^[36] This signifies that the gold atoms are closely packed. This is also confirmed by the XRD pattern of the gold film shown in **Figure 3**.

The crystalline structure of the 100 nm-thick gold film is shown in Figure 3. The reflection peaks were indexed using the standard inorganic crystal structure database pattern (ICSD PDF#89-3697 for gold and PDF#89-5012 for silicon).

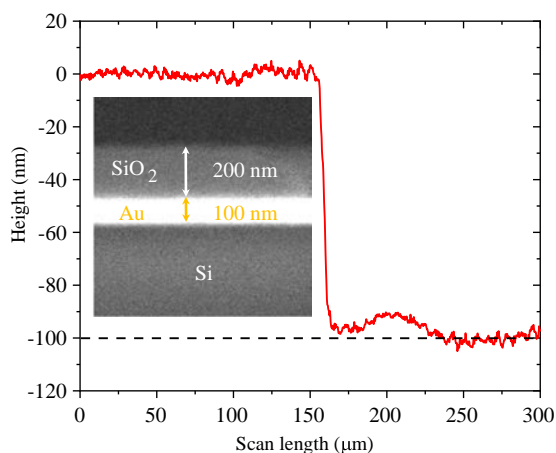


Figure 2. Step profile of the gold film on silicon. Inset: cross-sectional view of the gold film with 200 nm silicon oxide deposited atop.

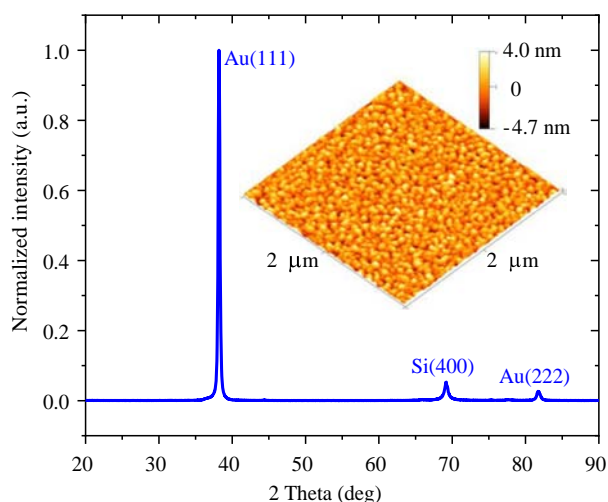


Figure 3. XRD pattern of the gold film on silicon. Inset: surface morphology of the gold film obtained by AFM.

The main peak Au(111) of gold is clearly identified. The average crystallite size could be estimated by Scherrer's equation,^[37] which is given by $D = 0.9\lambda/\beta\cos\theta$, where D is the average crystallite size, λ the wavelength of X-ray, β the line broadening at half the maximum intensity, and θ the Bragg angle. The estimated average crystallite size based on the Au(111) reflection peak is 29.7 nm.

The inset of Figure 3 illustrates the surface morphology of the gold surface measured by AFM, based on which the root-mean-square surface roughness is calculated to be 1.143 nm. This result is consistent with the roughness revealed by XRR, which is 1.60 ± 0.03 nm. The crystalline structure and surface morphology results shown in Figure 3 indicate that high-quality polycrystalline gold film with smooth surface was obtained. This kind of high-quality gold film with low surface roughness is crucial to the studying of the fluorescent behaviors of the dipole emitters deposited atop. The scattering effect due to surface roughness could be neglected. The resistivity of the gold film was measured

by a four-point probe. The bulk resistivity (in $\Omega\text{ cm}$) can be calculated by multiplying the sheet resistance (in $\Omega\text{ }\square^{-1}$) with the film thickness. The sheet resistance was measured to be $0.4015 \pm 0.0005\text{ }\Omega\text{ }\square^{-1}$, multiplying by the film thickness of 100 nm, yields the bulk resistivity of $4.015\text{ E-}6 \pm 5\text{ E-}9\text{ }\Omega\text{ cm}$. This result is consistent with the resistivity revealed by ellipsometry.

The optical properties of the gold and silicon oxide films were investigated by VASE. The dielectric function of the gold film is described by a Drude–Gaussian multioscillator model given by Equation (S1) and (S2), Supporting Information. The measured ellipsometric parameters (Psi and Delta) were compared with the modeling results using the CompleteEASE software. The goodness of fitting is quantified by the mean-squared-error (MSE) parameter, which is defined as the root mean squared difference between the measured and modeled functions of Psi and Delta. The measured and modeled Psi and Delta of the bare gold film before the deposition of silicon oxide film are shown in Figure 4a. The fitting parameters of the dielectric function of gold are shown in Table S1, Supporting Information. A best MSE as low as 3.407 has been achieved. The refractive index n and extinction coefficient k can be converted from the dielectric constants via $n = \left((\varepsilon_1' + \varepsilon_1'')^{1/2} / 2 + \varepsilon_1' / 2 \right)^{1/2}$ and $k = \left((\varepsilon_1' + \varepsilon_1'')^{1/2} / 2 - \varepsilon_1' / 2 \right)^{1/2}$, where ε_1' and ε_1'' are the real and imaginary part of the dielectric constant, respectively. The n and k of the gold film are plotted in Figure 4b and compared with the literature. Our result shows good agreement with these literatures: the result by Johnson et al.^[38] is obtained from reflection and transmission measurements of evaporated gold film with thickness of 34.3 and 45.6 nm on fused quartz substrate, while the result by Yakubovsky et al.^[39] is from ellipsometry measurements of evaporated gold film of 117 nm on silicon substrate. The correct determination of the refractive index of the gold film is important because the obtained results are submitted to the classical dipole model to determine the fluorescent lifetime and fluorescent intensity.

For the samples with different thicknesses of silicon oxide deposited on gold, a multiple sample analysis (MSA) has been applied to fit the ellipsometric results. The application of MSA can reduce the correlation between the fitting parameters.^[40] The optical constants of the gold film are assumed to be invariant for all the samples. For silicon and silicon oxide, the built-in dielectric functions in CompleteEASE were used. The ellipsometry fitting results are illustrated in Figure S2, Supporting Information. The best MSE obtained is 6.938. The obtained thicknesses of the silicon oxide films deposited on the gold surface show good agreement with that for the reference silicon pieces without gold film, as depicted in Figure S3, Supporting Information in the supporting information. The results demonstrated in this section indicate that high-quality gold films have been obtained. The various characterization methods give self-consistent results.

3.2. Fluorescence Lifetime Results

The fluorescence lifetimes of the Rhodamine molecules at different distances to the gold surface are measured by time-resolved

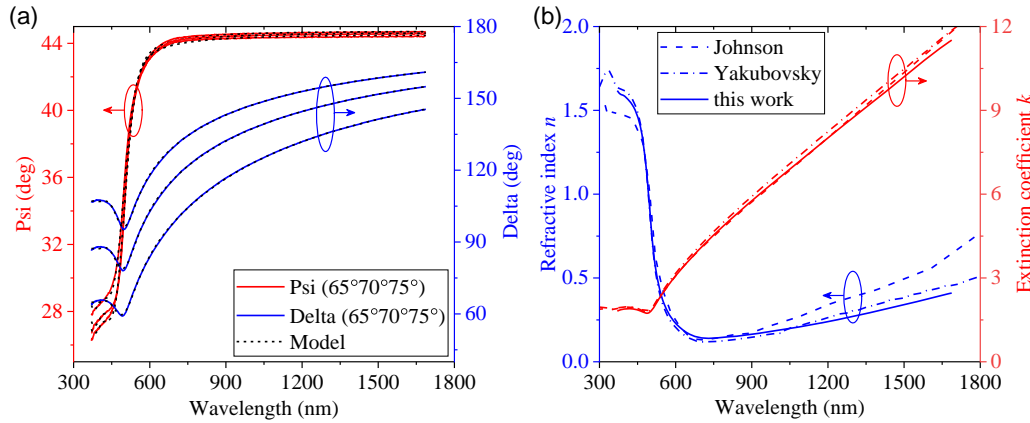


Figure 4. a) Fitting results of the ellipsometric parameters Psi and Delta for the 100 nm-thick gold film on silicon and b) comparison of refractive index and extinction coefficient of gold with literature.

fluorescence spectroscopy. A typical fluorescence decay curve is shown in Figure S4, Supporting Information. The measured fluorescence decay is the convolution of the idealized decay curve $F(t)$ and the instrument response function (IRF) of the detection system in the form of^[41]

$$I(t) = \int_{-\infty}^t F(t-t')\text{IRF}(t')dt' \quad (1)$$

We found that best fit can be obtained when the decay is given by the sum of two exponential functions $F(t) = A_1e^{-t/\tau_1} + A_2e^{-t/\tau_2}$, where A_1 and A_2 are the amplitude of the lifetime component τ_1 and τ_2 , respectively. The quality of fitting is given by the mean squared residual χ^2 . The fitting parameters of fluorescence decay curves for Rhodamine molecule at different distances d to the surface of gold and from a glass substrate are shown in Table S2, Supporting Information. The intensity averaged lifetime^[41] defined by

$\tau_{\text{int}} = (A_1\tau_1^2 + A_2\tau_2^2)/(A_1\tau_1 + A_2\tau_2)$ is used to compare with the classical dipole model, which treats the excited fluorescent molecules as forced and damped dipolar oscillators.^[20,22] The normalized damping rate of the dipole is given by

$$\frac{b}{b_0} = 1 + q\text{Re}\left(\frac{E_0}{E_s}\right) \quad (2)$$

where b_0 is the damping rate (inverse lifetime) in the absence of the surrounding structure, q the fluorescence quantum yield, E_0 the reflected field parallel to the dipole moment, and E_s a constant proportional to the strength of the dipole. For layered structures E_0 could be obtained by solving the Maxwell's equations with appropriate bounding conditions. The full expressions for the fluorescence lifetimes of a vertical electric dipole (VED) and a horizontal electric dipole (HED) are given by^[35]

$$\frac{\tau_0}{\tau_{\text{VED}}} = q\text{Re}\left(\frac{3}{2k_1^3} \int_0^\infty dk_\rho \frac{k_\rho^3}{k_{1x}} \left\{ \frac{[1 + r_{12}^{\text{TM}} \exp(i2k_{1x}d)][1 + r_{13}^{\text{TM}} \exp(i2k_{1x}s)]}{1 - r_{12}^{\text{TM}} r_{13}^{\text{TM}} \exp[i2k_{1x}(d+s)]} - 1 + \frac{1}{q} \right\}\right) \quad (3)$$

$$\frac{\tau_0}{\tau_{\text{HED}}} = q\text{Re}\left\{ \frac{3}{4k_1^3} \int_0^\infty dk_\rho k_{1x} k_\rho \left\{ \frac{[1 - r_{12}^{\text{TM}} \exp(i2k_{1x}d)][1 - r_{13}^{\text{TM}} \exp(i2k_{1x}s)]}{1 - r_{12}^{\text{TM}} r_{13}^{\text{TM}} \exp[i2k_{1x}(d+s)]} - 1 + \frac{1}{q} \right\} + \frac{3}{4k_1} \int_0^\infty dk_\rho \frac{k_\rho}{k_{1x}} \left\{ \frac{[1 + r_{12}^{\text{TE}} \exp(i2k_{1x}d)][1 + r_{13}^{\text{TE}} \exp(i2k_{1x}s)]}{1 - r_{12}^{\text{TE}} r_{13}^{\text{TE}} \exp[i2k_{1x}(d+s)]} - 1 + \frac{1}{q} \right\} \right\} \quad (4)$$

where τ_0 is the unquenched lifetime, q the fluorescence quantum yield, k_ρ and k_{ix} the in- and out-of-plane wavenumbers in region i , d and s the distance from the dipole to the gold surface and the air interface, respectively, and r_{ij}^{TE} and r_{ij}^{TM} the Fresnel reflection coefficients for the TE and TM waves at the interface between region i and region j , respectively.

The distance to gold surface and refractive index of gold determined by ellipsometry are submitted to Equation (3) and (4) to calculate the lifetimes for VED and HED. The unknown

parameters in these two equations are τ_0 and q , which can be obtained by fitting the modeled fluorescence lifetime results to the measured results. For isotropic (ISO) distribution of dipole orientations, the lifetime can be calculated from $1/\tau_{\text{ISO}} = 1/3\tau_{\text{VED}} + 2/3\tau_{\text{HED}}$. The measured fluorescence lifetime results are compared with the modeling results in Figure 5.

The curves shown in Figure 5 are the modeled lifetime results. The circles are the measured fluorescence lifetime results. It is clearly illustrated that the measured lifetimes can be best fitted by

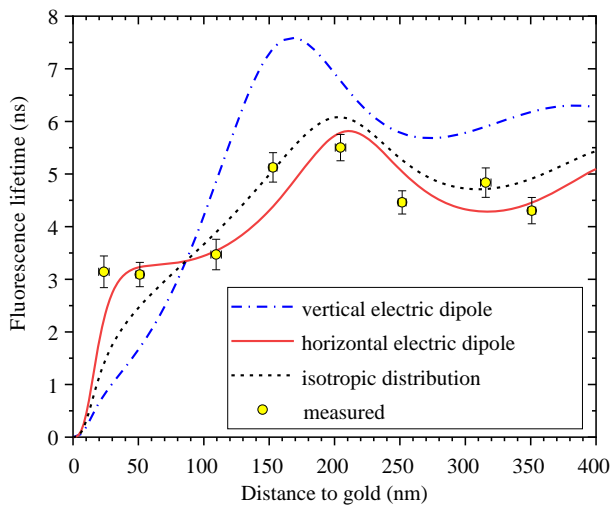


Figure 5. Fluorescence lifetime of Rhodamine molecule at different distance to the gold surface.

the dipolar model for a HED, with unquenched lifetime $\tau_0 = 4.6 \pm 0.1$ ns and fluorescence quantum yield $q = 0.9 \pm 0.05$. The revealed horizontal dipole orientation of Rhodamine 6G on silicon oxide surface is consistent with previous investigations.^[35,42,43] We measured the lifetime of Rhodamine 6G molecules prepared on a glass substrate to be 4.66 ± 0.11 ns via similar approach, which is close to the unquenched lifetime obtained by fitting with the dipole model. Similar fluorescent lifetime results of dipole emitters near metallic substrates have been obtained by the Langmuir–Blodgett technique.^[16,18] The result illustrated in Figure 5 demonstrates that the Rhodamine molecules prepared in experiments could be modeled as single dipole emitters. Due to the low concentration of the dye molecules in alcohol and the high-speed spin coating process, submonolayer of dye molecule was obtained. Similar observations have been reported in the literature.^[33,34] This conclusion could also be justified by the excellent match between the single dipole model and

the measured fluorescent intensity result shown in the next section, where we show that the fluorescence intensity of these single molecules could be modeled quantitatively by introducing the power spectrum of dipole emission. The result depicted in Figure 5 clearly indicates that the fluorescent lifetimes of the dye molecules have strong molecule–Au distance dependence. This phenomenon is discussed alongside the fluorescent emission intensity results in the following section.

3.3. Power Spectrum and Resonant Modes

The classical dipole model is comprehensive, but the key power dissipation channels are not unambiguous. Here, we apply the power spectrum for dipole emission introduced by Ford and Weber^[44] to analyze the waveguide (WG) modes and the surface plasmon polariton (SPP) modes supported by our layered sample structure. The total power P dissipated by a dipolar emitter is defined by a power spectrum of the in-plane wavenumber dP/dk_ρ via $P = \int_0^\infty dk_\rho (dP/dk_\rho)$. As P is the product of photon energy and the dipole damping rate, dP/dk_ρ is directly proportional to the integrand of the dipole damping rate given by Equation (3) or (4). The transverse electric (TE) and transverse magnetic (TM) power spectrum components for a HED are calculated from the two integrands in Equation (4) and plotted as a function of the distance to the gold film in Figure 6. Note that the abscissas for the power spectra are normalized by the wavenumber k_{10} in the dipole emitting layer, i.e., silicon oxide.

The WG modes and a SPP mode can be clearly identified in Figure 6 by the bright yellow lines. It is illustrated in Figure 6a that only a single TE mode is supported when the distance to gold is larger than approximately 50 nm. As the distance to gold increases to around 300 nm, another TE mode appears. The SPP mode is evidently depicted in Figure 6b by a white dashed line. As the distance to gold increases, the resonance frequency of the SPP mode approaches the frequency of the SPP mode supported by the interface of gold and silicon oxide of infinite thickness, which is given by $k_\rho = k_0 \sqrt{n_1^2 n_2^2 / (n_1^2 + n_2^2)}$, where n_1 and n_2 are the refractive index of silicon oxide and gold, respectively, and k_0 the wavenumber in vacuum.^[45] It is also shown in

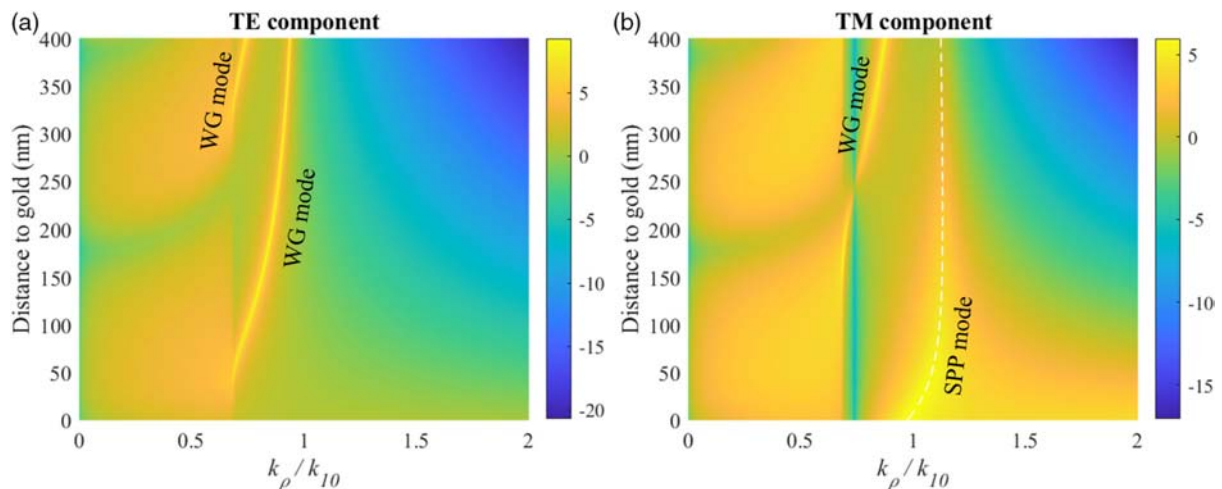


Figure 6. Power spectrum of a HED decomposed into the a) TE and b) TM components.

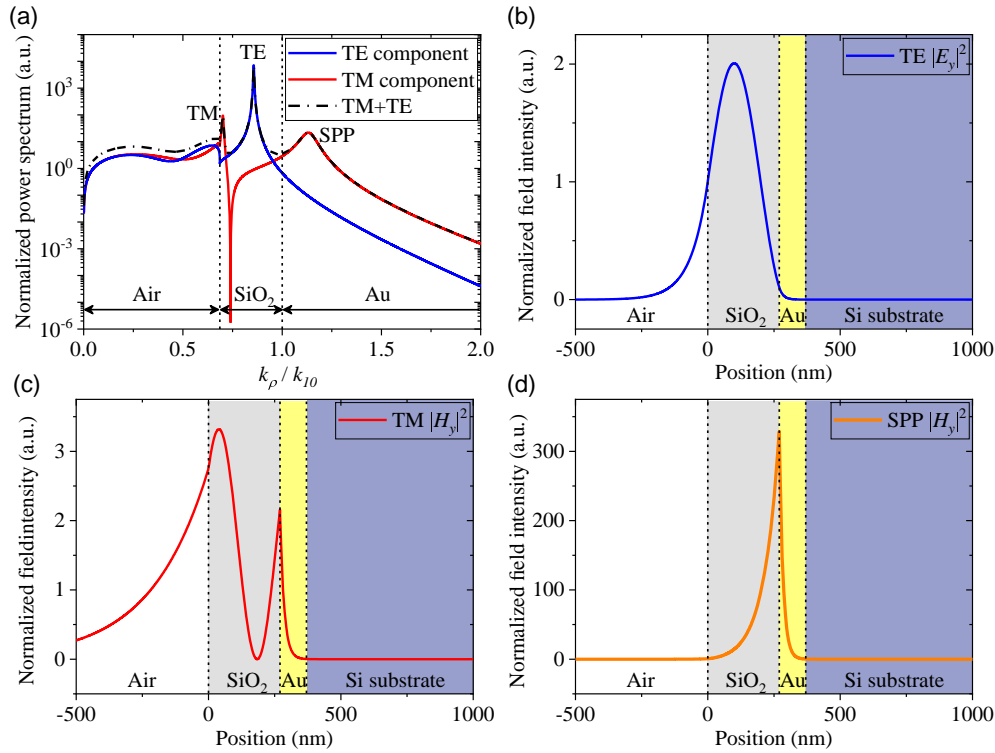


Figure 7. a) Normalized power spectrum at $d = 200$ nm and mode profile of b) TE WG, c) TM WG, and d) SPP modes.

Figure 6b that a TM WG mode emerges when the distance to gold is larger than 100 nm. The power spectrum shown in Figure 6 clearly illustrates the different power dissipation channels of the dipole radiation.

We take a slice from Figure 6, and plot the power spectrum when the distance to gold is 200 nm in **Figure 7a**. Three distinct peaks are identified in the power spectrum, which correspond to two WG modes and a SPP mode. The mode profile (normalized squared field intensity, $|E_y|^2$ and $|H_y|^2$ for TE and TM polarization, respectively) of these modes are calculated based on the transfer matrix method.^[45] Note that the coordinates are defined in the inset of Figure 1. The results are shown in Figure 7b–d. It is seen that the two WG waveguide modes are trapped in the silicon oxide layer by the air and the gold interface, whereas the SPP mode is trapped at the oxide–gold interface and the field intensity decreases monotonically away from this interface. The results shown in Figure 7 demonstrate the power dissipation channels of the dipole radiation, i.e., energy transfer to the various WG and SPP modes. In the next section, we quantify these channels by integrating the power spectrum in related wavenumber range.

3.4. Fluorescence Intensity Results

The dipole damping rate could be readily decomposed into different channels by evaluating the power spectrum dP/dk_p in respected wavenumber range.^[44,46] The radiated power in the far field can be obtained by integrating dP/dk_p in the range

$0 < k_p < k_{\text{Air}}$, the power trapped in the silicon oxide spacer layer can be obtained similarly in the range $k_{\text{Air}} < k_p < k_{\text{SiO}_2}$, and the power transferred to gold can be calculated in the range $k_p > k_{\text{SiO}_2}$, where k_{Air} and k_{SiO_2} are the wavenumbers in air and silicon oxide, respectively. The normalized power for a HED dissipated in these channels is plotted in **Figure 8a**.

It is seen from Figure 8a that the power transferred to metal decreases monotonically as the distance to gold increases. This part of power becomes negligible when the distance to gold is larger than 250 nm. Both of the power emitted in the far field and trapped in the silicon oxide layer oscillate in the whole distance range; their summation (as shown by the dashed curve in Figure 8a) contributes to the periodically oscillating behavior of the total power, which eventually converges to unity at large distance. The probability to detect fluorescence in the far field could be calculated from

$$\eta = \int_0^{k_{\text{Air}}} \frac{dP}{dk_p} dk_p / \int_0^\infty \frac{dP}{dk_p} dk_p \quad (5)$$

The fluorescence probabilities calculated at the emission wavelengths of 550, 600, and 650 nm by Equation (5) are compared with the measured fluorescence intensities at different distances to the gold surface in Figure 8b–d, respectively. Note that the fluorescence emission spectra for all the samples were measured under identical conditions, so the absolute fluorescence intensities are comparable. Fluorescence spectra of the

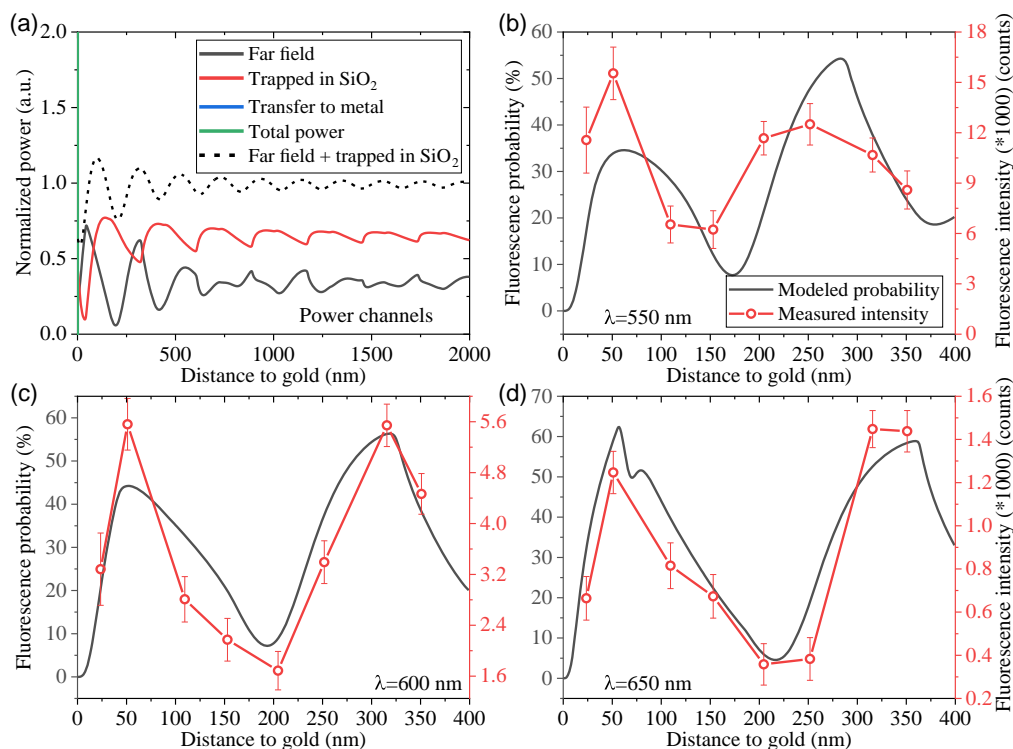


Figure 8. a) Dipole power dissipated in various channels for a HED. b–d) Comparison of modeled fluorescence probability (black solid curve) with measured fluorescence intensity (red circles) for emission wavelength at b) 550 nm, c) 600 nm, and d) 650 nm. The red solid lines connecting the circles are guides for the eye.

Rhodamine molecules at different distances to the surface of gold are shown in Figure S5, Supporting Information. It is clearly illustrated in Figure 8 that the modeled fluorescence probabilities fit well with the measured fluorescence intensity at different emission wavelengths. The results depicted in Figure 8 evidently demonstrate that the dipole model is able to predict the emission intensity of single molecules embedded in our layered optical structure. The power of the dipole radiation dissipated in the various channels, either the far field, the WG, or the SPP modes could be analytically calculated. For the stratified structure under investigation in this article, both the fluorescent lifetime and fluorescent emission intensity have strong molecule–Au distance dependence, as indicated by Figure 5 and 8. The fluorescent lifetime and intensity are modified by the competition of the different power dissipation channels upon the change of the molecule–Au distance. For the molecule–Au distance below 200 nm, the dominant power dissipation channels are energy transfer to the SPP mode and other lossy surface wave. Both the fluorescent lifetime and fluorescent intensity could be reduced significantly upon the excitation of these surface waves: as indicated in Figure 5, the fluorescent lifetime decreases monotonically as the interaction distance with these modes decreases; whereas the fluorescent intensity has a local maximum when the distance is around 50 nm, as illustrated in Figure 8. This is due to the periodic oscillation feature of the far field radiation via the interference effect of the source dipole radiation and

radiation reflected from the Au mirror. For the distance above 200 nm, the dominant power dissipation changed to be the far field radiation. Due to the aforementioned interference effect, the fluorescent lifetime and fluorescent intensity exhibit inverse periodic oscillations as the variation of the molecule–Au distance. In summary, the fluorescent lifetime and emission intensity have complex correlations as the variation of the molecule–Au distance, depending on whether the interaction is in the near field or the far field. However, the analytical modeling approach demonstrated in this article could be used to predict the fluorescent behavior quantitatively in both the near field and the far field interaction range. This approach represents a useful tool for the design and optimization of novel optoelectronic devices such as single-photon sources and delicate fluorescence spectroscopic systems incorporating dipole emitters.

4. Conclusion

We have investigated the fluorescence properties of Rhodamine 6G molecules at different distances to the surface of a high-quality gold film. The properties of the gold film have been characterized thoroughly by XRD(R), FESEM, profilometry, and ellipsometry. The TCSPC technique has been employed to study the time-resolved fluorescent property of the molecules. The fluorescence lifetime of the molecules as a function of their distance

to the surface of the gold film is well explained by a classical model for a horizontal electric dipole. The power dissipation channels of the dipole radiation are analyzed via its power spectrum of the in-plane wavenumber, based on which the probability to detect fluorescence in the far field has been calculated. We find that the calculated fluorescence probabilities at different distance to the gold surface show good agreement with the measured fluorescence intensities. The results presented in this article clearly demonstrate that the dipole model is able to predict the fluorescence lifetime as well as the fluorescence intensity of single molecules embedded in layered optical environments. Further investigations for more complicated plasmonic platforms could be developed based on the modeling approach described in this article. Our investigation is important to the understanding of the fluorescent behavior of dipole-like emitters near the surface of metals, and paves way for the design and optimization of novel optoelectronic devices employing dipole emitters, complex plasmonic nanostructures, and emerging low-dimensional materials.

Supporting Information

Supporting Information is available from the Wiley Online Library or from the author.

Acknowledgements

The authors would like to acknowledge the financial support from the Program for Guangdong Introducing Innovative and Entrepreneurial Teams (grant no. 2019ZT08L101) and the National Natural Science Foundation of China (grant no. 61604138). Experiments were performed partly using the tools maintained by Southern University of Science and Technology Core Research Facilities. The authors are grateful to Dr. A. Batalov for kind help with fluorescence measurements, and Dr. L. Danos and Prof. T. Markvart for careful reading of the manuscript.

Conflict of Interest

The authors declare no conflict of interest.

Data Availability Statement

The data that support the findings of this study are available from the corresponding author upon reasonable request.

Keywords

energy transfer, fluorescence, lifetime, plasmonics, waveguides

Received: January 18, 2022

Revised: April 5, 2022

Published online: April 15, 2022

- [1] R. Chikkaraddy, B. de Nijs, F. Benz, S. J. Barrow, O. A. Scherman, E. Rosta, A. Demetriadou, P. Fox, O. Hess, J. J. Baumberg, *Nature* **2016**, 535, 127.
 [2] N. Nikolay, N. Mendelson, E. Özelci, B. Sontheimer, F. Böhm, G. Kewes, M. Toth, I. Aharonovich, O. Benson, *Optica* **2019**, 6, 1084.

- [3] G. Zhang, H. Liu, S. Jia, H. Li, Z. Li, Q. Gong, J. Chen, *Adv. Quantum Technol.* **2020**, 3, 2000033.
 [4] Y. Wu, X. Liu, X. Qi, L. Lu, G. Guo, G. Guo, X. Ren, *Appl. Phys. Lett.* **2021**, 118, 104002.
 [5] J. R. Lakowicz, K. Ray, M. Chowdhury, H. Szmajda, Y. Fu, J. Zhang, K. Nowaczyk, *Analyst* **2008**, 133, 1308.
 [6] W. Deng, E. M. Goldys, *Langmuir* **2012**, 28, 10152.
 [7] J. Dong, S. Qu, Z. Zhang, M. Liu, G. Liu, X. Yan, H. Zheng, *J. Appl. Phys.* **2012**, 111, 093101.
 [8] D. Darvill, A. Centeno, F. Xie, *Phys. Chem. Chem. Phys.* **2013**, 15, 15709.
 [9] C. Joyce, S. M. Fothergill, F. Xie, *Mater. Today Adv.* **2020**, 7, 100073.
 [10] S. A. Maier, H. A. Atwater, *J. Appl. Phys.* **2005**, 98, 011101.
 [11] E. Cao, W. Lin, M. Sun, W. Liang, Y. Song, *Nanophotonics* **2018**, 7, 145.
 [12] M. R. Gonçalves, H. Minassian, A. Melikyan, *J. Phys. D: Appl. Phys.* **2020**, 53, 443002.
 [13] E. Takeda, M. Fujii, T. Nakamura, Y. Mochizuki, S. Hayashi, *J. Appl. Phys.* **2007**, 102, 023506.
 [14] Y. Mochizuki, M. Fujii, S. Hayashi, T. Tsuruoka, K. Akamatsu, *J. Appl. Phys.* **2009**, 106, 013517.
 [15] H. F. Arnoldus, Z. Xu, X. Li, *J. Appl. Phys.* **2020**, 127, 083101.
 [16] K. H. Drexhage, *Prog. Opt.* **1974**, 12, 163.
 [17] L. Danos, T. Markvart, *Chem. Phys. Lett.* **2010**, 490, 194.
 [18] L. Fang, K. S. Kiang, N. P. Alderman, L. Danos, T. Markvart, *Opt. Express* **2015**, 23, A1528.
 [19] L. Danos, N. R. Halcovitch, B. Wood, H. Banks, M. P. Coogan, N. Alderman, L. Fang, B. Dzurak, T. Markvart, *Faraday Discuss.* **2020**, 222, 405.
 [20] R. R. Chance, A. Prock, R. Silbey, *Adv. Chem. Phys.* **1978**, 37, 1.
 [21] L. Novotny, B. Hecht, *Principles of Nano-optics*, Cambridge University Press, Cambridge **2006**.
 [22] W. L. Barnes, *J. Mod. Opt.* **1998**, 45, 661.
 [23] B. van Dam, C. I. Osorio, M. A. Hink, R. Muller, A. F. Koenderink, K. Dohnalova, *ACS Photonics* **2018**, 5, 2129.
 [24] E. Özelci, B. Rühle, F. Weigert, B. Lubotzky, G. Kewes, U. Resch-Genger, O. Benson, *J. Phys. Chem. C* **2019**, 123, 20468.
 [25] G. Gómez-Santos, T. Stauber, *Phys. Rev. B* **2011**, 84, 165438.
 [26] N. Karedla, A. I. Chizhik, I. Gregor, A. M. Chizhik, O. Schulz, J. Enderlein, *ChemPhysChem* **2014**, 15, 705.
 [27] R. J. Moerland, J. P. Hoogenboom, *Optica* **2016**, 3, 112.
 [28] A. Ghosh, A. Sharma, A. I. Chizhik, S. Isbaner, D. Ruhlandt, R. Tsukanov, I. Gregor, N. Karedla, J. Enderlein, *Nat. Photonics* **2019**, 13, 860.
 [29] A. Ghosh, A. I. Chizhik, N. Karedla, J. Enderlein, *Nat. Protoc.* **2021**, 16, 3695.
 [30] H. Huang, F. Deng, J. Xiang, S. Li, S. Lan, *Appl. Surf. Sci.* **2021**, 542, 148660.
 [31] A. O. Hamza, F. N. Viscomi, J.-S. G. Bouillard, A. M. Adawi, *J. Phys. Chem. Lett.* **2021**, 12, 1507.
 [32] M. Hertzog, B. Munkhbat, D. Baranov, T. Shegai, K. Börjesson, *Nano Lett.* **2021**, 21, 1320.
 [33] T. F. Heinz, C. K. Chen, D. Ricard, Y. R. Shen, *Phys. Rev. Lett.* **1982**, 48, 478.
 [34] W. P. Ambrose, P. M. Goodwin, J. C. Martin, R. A. Keller, *Phys. Rev. Lett.* **1994**, 72, 160.
 [35] L. Fang, L. Danos, T. Markvart, R. Chen, *Opt. Lett.* **2020**, 45, 4618.
 [36] D. R. Lide, *CRC Handbook of Chemistry and Physics*, CRC Press, Boca Raton **2004**.
 [37] A. L. Patterson, *Phys. Rev.* **1939**, 56, 978.
 [38] P. B. Johnson, R. W. Christy, *Phys. Rev. B* **1972**, 6, 4370.
 [39] D. I. Yakubovsky, A. V. Arsenin, Y. V. Stebunov, D. Y. Fedyanin, V. S. Volkov, *Opt. Express* **2017**, 25, 25574.

- [40] J. N. Hilfiker, N. Singh, T. Tiwald, D. Convey, S. M. Smith, J. H. Baker, H. G. Tompkins, *Thin Solid Films* **2008**, 516, 7979.
- [41] J. R. Lakowicz, *Principles of Fluorescence Spectroscopy*, Springer, Berlin **2006**.
- [42] H. Sano, G. Mizutani, S. Ushioda, *Surf. Sci.* **1989**, 223, 621.
- [43] G. Crossen, K. E. Drabe, D. A. Wiersma, *J. Chem. Phys.* **1993**, 98, 5276.
- [44] G. W. Ford, W. H. Weber, *Phys. Rep.* **1984**, 113, 195.
- [45] P. Yeh, *Optical Waves in Layered Media*, Wiley, Hoboken, NJ **2005**.
- [46] B. J. Soller, D. G. Hall, *J. Opt. Soc. Am. A* **2001**, 18, 2577.